Journal of Magnetic Resonance **153,** 267–272 (2001)
doi:10.1006/jmre.2001.2449, available online at http://www.idealibrary.com on IDEAL®

COMMUNICATIONS

Two Simple NMR Experiments for Measuring Dipolar Couplings in Asparagine and Glutamine Side Chains

Perttu Permi

Institute of Biotechnology, University of Helsinki, P.O. Box 56, FIN-00014, Helsinki, Finland

E-mail: Perttu.Permi@helsinki.fi

Received June 18, 2001; revised September 17, 2001; published online November 7, 2001

Residual dipolar couplings are now widely used for structure determination of biological macromolecules. Until recently, the main focus has been on measurement of dipolar couplings in the protein main chain. However, with the aim of more complete protein structure, it is also essential to have information on the orientation of protein side chains. In addition, residual dipolar couplings can potentially be employed to study molecular dynamics. In this Communication, two simple NH_2 and spin-state edited experiments are presented for rapid and convenient determination of five residual dipolar couplings from ^{15}N, ^{1}H correlation spectrum in asparagine and glutamine side chains. The pulse sequences are demonstrated on two proteins, 30.4-kDa Cel6A in diluted liquid crystal phase and 18-kDa human cardiac troponin C in water.

Key Words: **cardiac troponin C; Cel6A; HSQC; NMR; residual dipolar couplings; side chains; spin-state selective filters.**

NMR spectroscopic structure determination of biological macromolecules has been under rapid development during the past 20 years. One of the latest milestones was the introduction of residual dipolar couplings as a means for structure determination of proteins and nucleic acids (*1–3*). Residual dipolar couplings, which originate from anisotropic tumbling of molecules in dilute liquid crystals, can be used for improved definition of molecular structures or for recognition of protein folds (*4–7*). As magnitude and sign of dipolar couplings depend on the orientation of the internuclear vector with respect to the magnetic field, dipolar couplings serve as truly range independent restraints in structure determination of biomolecules. The level of alignment can be tuned by altering the concentration of the liquid crystal medium enabling the measurement of inherently smaller dipolar couplings, in addition to $^{1}D_{CH}$ and $^{1}D_{NH}$ (*2, 3, 6*). Measurement of several dipolar couplings per residue allows the accurate estimation of the principle components of the alignment tensor (*5*) and effectively averages the nonlinear response of each individual dipolar coupling with respect to the polar angles (*8*).

Due to the enormous potential of the structural restraints derived from dipolar couplings, a number of experiments have been designed for precise and convenient measurement of couplings in $^{15}N/(^{2}H)$- and $^{15}N/^{13}C/(^{2}H)$-labeled proteins. The main focus has been on the measurement of dipolar interactions between nuclei in the protein backbone (*8–15*). Recently emphasis has been shifting toward protein side chains, in order to obtain information on their orientation and conformational space (*16–22*). In addition, dipolar couplings can potentially be used for studying molecular dynamics because methods for measuring dipolar couplings are sensitive to molecular motions ensuing on time scales shorter than 100 ms (*23, 24*). In this respect the measurement of dipolar couplings in protein side chains is crucial for attaining arrant molecular structures and studying of molecular behaviour.

We have favored simplified two-dimensional ^{15}N, ^{1}H correlation spectra for measuring main-chain dipolar couplings (*13–15*). However, for large proteins three-dimensional experiments are preferred, due to spectral crowding (*8, 11, 12*). For side-chain NH_2 moieties found in asparagine and glutamine residues, two-dimensional ^{15}N, ^{1}H correlation spectra are often adequate and very practical. In this Communication we present two sensitive, NH_2 edited, (double) spin-state-selective NMR experiments for measuring $^{1}J_{H^{N}N}$ ($^{1}J_{NCO}$ and $^{2}J_{H^{N}CO}$) couplings in Asn and Gln side chains. The proposed experiments provide information on the orientation of five internuclear vectors in the form of $^{1}H^{N1}$–^{15}N, $^{1}H^{N2}$–^{15}N, $^{1}H^{N1}$–^{13}CO, $^{1}H^{N2}$–^{13}CO, and ^{15}N–^{13}CO couplings, which enables one to assess the orientation and study the dynamics of the Asn and Gln residues in $^{15}N/(^{2}H)$- or $^{15}N/^{13}C/(^{2}H)$-enriched protein samples.

The H_2N–HSQC–α/β–J pulse sequence depicted in Fig. 1a can be used for measuring one-bond ^{15}N–^{1}H couplings in the NH_2 moieties in $^{15}N/(^{2}H)$-labeled proteins. The pulse sequence is based on a familiar ^{15}N HSQC experiment (*25*) but it employs a novel NH_2 editing, and spin-state selection (*26–28*) with respect to the ^{15}N spin in the F_2 dimension, for convenient and rapid determination of the $^{1}J_{H^{N}N}$ and $^{1}D_{H^{N}N}$ couplings in Asn and Gln residues. In the presented pulse scheme, the proton magnetization is initially transferred to nitrogen. Subsequently the desired

1090-7807/01 $35.00

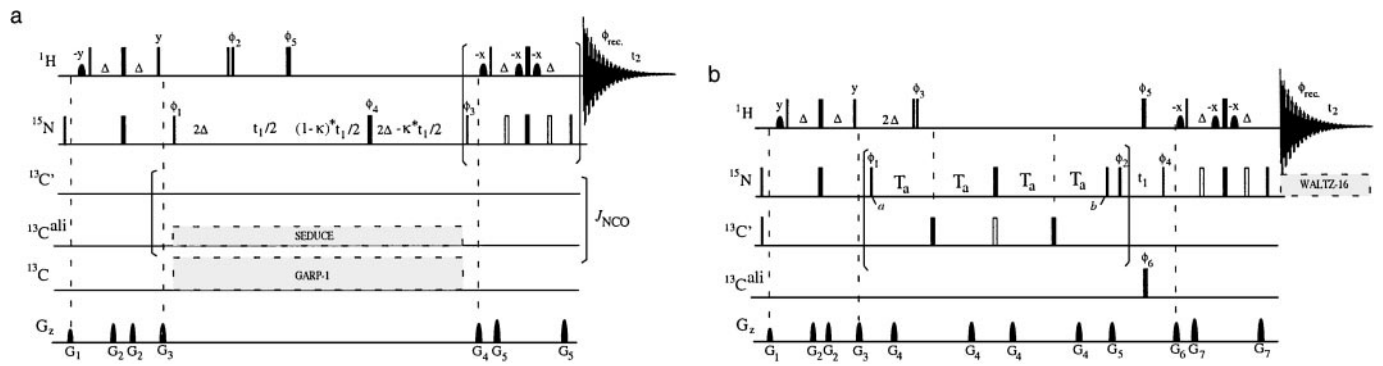

FIG. 1. The H_2N–HSQC–α/β–J pulse sequence (a) for determination of scalar and residual dipolar ^{15}N–^{1}H couplings from simplified two-dimensional NH_2 edited ^{15}N–^{1}H correlation spectra in Asn and Gln side chains. Narrow (wide) bars denote 90° (180°) pulses, with phase x unless otherwise indicated. Half-ellipses describe water selective 90° pulses to obtain water-flip-back (*36, 37*). All 180° pulses for $^{13}C'$ and $^{13}C^{ali}$ are 333-μs band-selective G3 inversion pulses (*38*) applied at the center of $^{13}C'$ (176 ppm) and $^{13}C^{ali}$ (35 ppm) regions. The ^{1}H, ^{15}N, $^{13}C'$, and $^{13}C^{ali}$ carrier positions are 4.7 (water), 120 (center of ^{15}N spectral region), 176 ppm (center of $^{13}C'$ spectral region), and 35 ppm (center of aliphatic ^{13}C spectral region), respectively. The delays employed are $\Delta = 1/(4J_{NH})$; $0 \le \kappa \le (2\Delta)/t_{1,max}$. Phase cycling: $\phi_1 = x$; $\phi_2 = x, -x$; $\phi_3 = 2(x), 2(-x)$; $\phi_4 = 4(x), 4(y)$; $\phi_5 = 8(x), 8(-x)$; $\phi_{rec.} = x, 2(-x), x, -x, 2(x), -x$. For the in-phase spectrum filled 180° and 90° pulses are applied during the filter, whereas for the antiphase spectrum two unfilled 180° pulses are applied. Quadrature detection in the F_1 dimension is obtained by altering the phase of ϕ_1 according to States-TPPI (*39*). The resolution and sensitivity in the ^{15}N dimension is improved by implementing the ^{15}N chemical shift evolution in a semiconstant time manner (*29, 30*). If the pulse scheme is used for simultaneous determination of ^{15}N–^{13}CO and $^{1}H^{N}$–^{13}CO couplings, the ^{13}C decoupling should be replaced by the semiselective $^{13}C^{ali}$ decoupling scheme (*40*). Pulsed field gradients are inserted as indicated for the suppression of the undesired coherence pathways and residual water suppression. Strengths and durations of gradients are $G_1 = (0.5$ ms, 4 G/cm), $G_2 = (0.7$ ms, 18.5 G/cm), $G_3 = (0.5$ ms, 7 G/cm), $G_4 = (0.5$ ms, 9 G/cm), $G_5 = (0.3$ ms, −13.3 G/cm). Due to 90° phase difference between the in-phase and antiphase spectrum, the real and imaginary parts must be interchanged in either the in- or antiphase data set prior to addition and subtraction of the data sets. (b) The $H_2N(\alpha/\beta$–HNCO–$J)$ scheme for measuring ^{13}CO–^{15}N, $^{1}H^{N}$–^{13}CO (and ^{15}N–^{1}H) couplings in Asn and Gln side chains. All parameters as in the scheme (a) except $T_a = 1/(8J_{NC'})$. Phase cycling for the in-phase spectrum (filled 180° pulses are applied on $^{13}C'$) with respect to $^{1}J_{NCO}$ $\phi_1 = x$; $\phi_2 = x, -x$; $\phi_3 = 2(x), 2(-x)$; $\phi_4 = 4(x), 4(-x)$; $\phi_5 = 8(x), 8(-x)$; $\phi_6 = 16(x), 16(-x)$; $\phi_{rec.} = x, 2(-x)\ x, -x, 2(x), -x$; for the antiphase spectrum (unfilled 180° pulse is applied for $^{13}C'$): $\phi_1 = y$. If $^{1}J_{H^{N}N}$ is measured simultaneously in F_2 using the spin-state selection, additional in- and antiphase spectra with respect to $^{1}J_{H^{N}N}$ are recorded as in the scheme (a). Otherwise in-phase filter and subsequent ^{15}N decoupling are applied. The gradient strengths and durations are $G_1 = (0.5$ ms, 4 G/cm), $G_2 = (0.7$ ms, 18.5 G/cm), $G_3 = (0.5$ ms, 7 G/cm), $G_4 = (0.8$ ms, 9 G/cm), $G_5 = (0.5$ ms, −12.8 G/cm), $G_6 = (0.3$ ms, 5.7 G/cm), $G_7 = (0.3$ ms, −13.3 G/cm). For each scheme, the in- and antiphase data are recorded in an interleaved manner and subsequently added and subtracted to separate the multiplet components to two or four subspectra.

magnetization described by the density operator $2H^{N1}{}_zN_y$, arising from the NH_2 groups, remains antiphase with respect to one of the amide protons (conversion from $2H^{N1}{}_zN_y$ to $2H^{N2}{}_zN_y$) after the first order filtering period ($2\Delta = 1/(2J_{H^{N}N})$). Two 90° ($^{1}H$) pulses ensure selection of the coherence, which is antiphase with respect to proton. Therefore the magnetization originating on NH_2 moieties passes through the filter, whereas the filter efficiently purges the magnetization initially residing in the amides of the protein backbone. The ^{15}N chemical-shift evolution is labeled during the following t_1 period, which is inserted into the pulse sequence in a semi-constant-time manner (*29, 30*) for improved sensitivity and resolution. The second 2Δ period acts, in fact, as a second order J filter. The magnetization arising from the main-chain amides, which leaks through the first J filter ($2H^{N}{}_zN_y \cos(2\pi J_{H^{N}N}\Delta)$), will be diminished further by this second filter element ($2H^{N}{}_zN_y \cos^2(2\pi J_{H^{N}N}\Delta)$). In contrast, the desired magnetization from the NH_2 side chains will remain antiphase with respect to one of the directly bonded protons (conversion from $2H^{N2}{}_zN_y$ back to $2H^{N1}{}_zN_y$).

After the NH_2 editing and the ^{15}N chemical-shift labeling period, the magnetization is transferred back to protons $2H^{N1}{}_yN_z$. The unnecessary spectral crowding due to the one-bond ^{15}N–^{1}H coupling during acquisition can be avoided by spin-state selection. Thus, the in-phase and antiphase filter periods replace the refocusing INEPT period. These two experiments are referred to here as the in-phase and the antiphase experiments, respectively. In the in-phase experiment, the $2H^{N1}{}_yN_z$ magnetization that is antiphase with respect to ^{15}N evolves into in-phase $H^{N1}{}_x$ coherence during the in-phase filter element (depicted with filled 180° and 90° pulses on ^{15}N). The final 90° pulse on nitrogen removes the undesired dispersive contribution ($2H^{N1}{}_yN_z$) resulting from J-mismatch. In contrast, in the antiphase experiment, the magnetization remains antiphase after passing through the antiphase filter element (described with unfilled 180° pulses on ^{15}N) since the ^{15}N–^{1}H coupling is efficiently eliminated during the filter. Both filter elements (*28*) average the cross-correlation between dipole–dipole and chemical shielding anisotropy relaxation mechanisms (*31*). Although it is possible to use IPAP-style (*9*) filtering (i.e., for which the filtering block for the creation of the antiphase magnetization can be removed), we favor the principle described above in order to achieve identical water suppression in both filter elements. Addition and subtraction of the corresponding in-phase and antiphase data sets result in two NH_2 correlation spectra with cross peaks at (ω_N, $\omega_{H^{N1}} - \pi\,{}^{1}J_{H^{N1}N}$

and ω_N, $\omega_{H^{N1}} + \pi\,{}^1J_{H^{N1}N}$), and ($\omega_N$, $\omega_{H^{N2}} - \pi\,{}^1J_{H^{N2}N}$ and ω_N, $\omega_{H^{N2}} + \pi\,{}^1J_{H^{N2}N}$) for $^1H^{N1}$–^{15}N and $^1H^{N2}$–^{15}N correlations, respectively. Thus, $^1J_{H^{N1}N}$ and $^1J_{H^{N2}N}$ can be measured from the frequency difference in the F_2 dimension between two spectra for the $^1H^{N1}$–^{15}N and $^1H^{N2}$–^{15}N correlations, respectively.

In the anisotropic phase where dipolar couplings may contribute 20–30 Hz to the one-bond ^{15}N–^1H couplings, some of the undesired magnetization of the main-chain signals will leak through the NH_2 filters, resulting in incomplete cancellation of the backbone amide signals (*vide supra*). For the NH_2 moieties, the filtering performance is excellent given that the desired transfer pathway from antiphase $H^{N1}{}_zN_y$ via $H^{N2}{}_zN_y$ to $H^{N1}{}_zN_y$ coherence has $\sin^2(2\pi J_{H^{N1}N}\Delta)\sin^2(2\pi J_{H^{N2}N}\Delta)$ dependence, whereas the undesired from/to $H^{N1}{}_zN_y$ transfer has $\cos^2(2\pi J_{H^{N1}N}\Delta)\cos^2(2\pi J_{H^{N2}N}\Delta)$ dependence on signal intensity. Consequently, the main-chain amide signals are attenuated by $\sin^2(2\pi J_{H^{N1}N}\Delta)\sin^2(2\pi J_{H^{N2}N}\Delta)/\cos^2(2\pi J_{H^NN}\Delta)$ and the undesired NH_2 transfer pathway by $\sin^2(2\pi J_{H^{N1}N}\Delta)\sin^2(2\pi J_{H^{N2}N}\Delta)/\cos^2(2\pi J_{H^{N1}N}\Delta)\cos^2(2\pi J_{H^{N2}N}\Delta)$ with respect to the preferred NH_2 correlations in the resulting spectrum.

Concerning the spin-state-selection filtering, the filter tuned to $1/(2J_{H^NN})$ is rather insensitive to variations in the $^1J_{H^NN}$ coupling values (94 ± 25 Hz, $<3\%$ leakage) as has been discussed earlier (*9, 13*). The influence of incomplete suppression of the undesired multiplet components on the measurement of the coupling constants has been discussed previously (*8, 13, 14, 32*) and will not be elaborated further here.

One caveat of the proposed experiment stems from the fact that large homonuclear dipolar interactions may complicate measurement of couplings from the proton dimension. However, in the case of NH_2 moieties the measurement of individual $^1J_{H^NN}$ couplings can be accomplished more easily in the proton dimension than in the nitrogen dimension, where the $^1J_{H^{N1}N}$ and $^1J_{H^{N2}N}$ couplings are quite similar in size with respect to the ^{15}N linewidth. Consequently, the $\alpha\beta$- and $\beta\alpha$-components of the doublet of doublets overlap, preventing accurate measurement of these couplings in the frequency domain. Moreover, the use of perdeuterated samples reduces unresolved homonuclear dipolar couplings in side-chain amides to a minimum, and consequently the vital contribution to linewidth arises from the geminal proton pair itself, the information that can be useful itself.

It is worth mentioning that the H_2N–HSQC–α/β–J experiment can be simultaneously used for measuring also $^1J_{NCO}$ and $^2J_{H^NCO}$ couplings in $^{15}N/^{13}C/(^2H)$-labeled samples by simply replacing the broadband ^{13}C decoupling, during the period nitrogen is in transverse plane ($4\Delta + t_1$), with the semiselective $^{13}C^{ali}$ decoupling. Thus, the coupling between ^{15}N and ^{13}CO evolves during t_1. However, this increases the number of peaks in the spectrum by a factor of 2 and thus may become an issue in large proteins. Furthermore, if the $^1J_{NCO}$ doublets are not resolved to baseline, the measured couplings are underestimates of their true value (*13*). Therefore, it is advantageous to make use of the spin-state selection for measuring $^1J_{NCO}$ and $^2J_{H^NCO}$ especially with larger proteins.

The $H_2N(\alpha/\beta$–HNCO–$J)$ pulse sequence, used for the simultaneous measurement of the one-bond ^{15}N–^1H, ^{15}N–^{13}CO and two-bond $^1H^N$–^{13}CO couplings in $^{15}N/^{13}C/(^2H)$-enriched protein samples, is illustrated in Fig. 1b. The pulse sequence is based on the HN(α/β–NC'–J) experiment devised for measuring one-bond ^{15}N–$^{13}C'$ and two-bond $^1H^N$–$^{13}C'$ couplings in the protein backbone (*13*). First the magnetization is transferred from amide protons to their directly bound nitrogen. The following second-order NH_2 editing analogous to the H_2N–HSQC–α/β–J experiment, with simultaneous spin-state selection relative to the adjacent carbonyl carbon, enables separation of the NH_2 signals from the main-chain amides and measurement of the ^{15}N–^{13}CO and $^1H^N$–^{13}CO couplings from two subspectra each containing only a single set of NH_2 correlations. Thus, starting from the antiphase $2H^{N1}{}_zN_x$ magnetization (time point *a*), the desired pathway during the antiphase filter element (a 180° pulse denoted by an unfilled bar is applied on ^{13}CO after the delay $2T_a$) leads to $4H^{N1}{}_zN_yCO_z$ coherence (time point *b*). The coupling between ^{15}N and ^{13}CO is removed during the in-phase filter element (two 180° pulses denoted by filled bars are applied on ^{13}CO) and, as a result, the initial $2H^{N1}{}_zN_y$ coherence evolves into $2H^{N1}{}_zN_y$ (time point *b*). The subsequent pulsed field gradient (PFG) z-filter purges the undesired magnetization components, while the desired components are transformed into the transverse plane prior to the t_1 period. During t_1, the ^{15}N chemical shift evolves simultaneously with its coupling to the ^{13}CO spin and ultimately the desired magnetization is brought back to proton. Thus, the relevant terms for the in-phase and antiphase experiments can be described by the density operators $2H^{N1}{}_yN_z\cos(\pi J_{NC},t_1)\cos(\omega_Nt_1)$ and $4H^{N1}{}_yN_zCO_z\sin(\pi J_{NC},t_1)\sin(\omega_Nt_1)$ and $4H^{N1}{}_yN_zCO_z\cos(\pi J_{NC},t_1)\cos(\omega_Nt_1)$ and $2H^{N1}{}_yN_z\sin(\pi J_{NC},t_1)\sin(\omega_Nt_1)$ prior to the reverse-INEPT, respectively. If the simultaneous measurement of ^{15}N–^1H couplings is preferred, spin-state-selective filtering similar to Fig. 1a can be used. This can be very useful in the case of unstable samples, which are unable to preserve identical alignment for long periods (*33*). Alternatively, the in-phase filter element can be used with simultaneous decoupling of ^{15}N during acquisition (marked with a dashed box during acquisition). It is worth pointing out that although the signal-to-noise ratio is smaller for the ^{15}N-coupled version of the experiment, the number of measurements for each coupling (2 for $^1J_{H^NN}$ and $^2J_{H^NCO}$, 4 for $^1J_{NCO}$) will partly compensate for this. In other words, the loss in S/N will be somewhat reimbursed by averaging the random error; i.e., the net loss is $\sqrt{2}/2$. The appropriate addition and subtraction of two (four, if spin-state selection is used for measuring $^1J_{H^NN}$) data sets result in two (four) subspectra with correlations occurring at $\omega_N + \pi\,{}^1J_{NCO}$, $\omega_{H^{N1}} + \pi^2J_{H^{N1}CO}$ and $\omega_N - \pi\,{}^1J_{NCO}$, $\omega_{H}N1 - \pi^2J_{H^{N1}CO}$ ($\omega_N + \pi\,{}^1J_{NCO}$, $\omega_{H^{N1}} + \pi^2J_{H^{N1}CO} + \pi\,{}^1J_{H^{N1}N}$; $\omega_N + \pi\,{}^1J_{NCO}$, $\omega_{H^{N1}} + \pi^2J_{H^{N1}CO} - \pi\,{}^1J_{H^{N1}N}$; $\omega_N - \pi\,{}^1J_{NCO}$, $\omega_H1 - \pi^2J_{H^{N1}CO} + \pi\,{}^1J_{H^{N1}N}$ and $\omega_N - \pi\,{}^1J_{NCO}$, $\omega_{H^{N1}} - \pi^2J_{H^{N1}CO} - \pi\,{}^1J_{H^{N1}N}$). Correlations for $^1H^{N2}$ can be described analogously. Thus, the $^1J_{NCO}$ couplings can be measured from cross-peak displacements

in the ^{15}N dimension between two subspectra. Two-bond $^{2}J_{H^{N}CO}$ couplings can be measured in the same way from the cross-peak displacement in the proton dimension between two subspectra. If additional spin-state selection in t_2 is used, the one-bond coupling between ^{15}N and ^{1}H can be obtained by comparing averaged frequencies of $\omega_N + \pi\,^{1}J_{NCO}$, $\omega_{H^{N1}} + \pi\,^{2}J_{H^{N1}CO} + \pi\,^{1}J_{H^{N1}N}$ and $\omega_N + \pi\,^{1}J_{NCO}$, $\omega_{H^{N1}} - \pi\,^{2}J_{H^{N1}CO} + \pi\,^{1}J_{H^{N1}N}$ with $\omega_N + \pi\,^{1}J_{NCO}$, $\omega_{H^{N1}} + \pi\,^{2}J_{H^{N1}CO} - \pi\,^{1}J_{H^{N1}N}$ and $\omega_N + \pi\,^{1}J_{NCO}$, $\omega_{H^{N1}} - \pi\,^{2}J_{H^{N1}CO} - \pi\,^{1}J_{H^{N1}N}$ subspectra in the proton dimension. The same approach applies to $^{1}J_{NCO}$ and $^{2}J_{H^{N}CO}$ also. It is noteworthy that determination of $^{1}J_{NCO}$ is based on four independent measurements.

As mentioned previously, the spin-state selection with filter length adjusted to $1/(2J)$ is rather insensitive to J-leakage. However, in the anisotropic phase clean separation of multiplet components is not always achieved for all residues due to large dipolar contributions. In the proposed $H_2N(\alpha/\beta$–HNCO–$J)$ experiment, the undesired magnetization hampering the measurement arises in practice from two sources (if the sequence is used for measuring one-bond ^{15}N–^{1}H couplings simultaneously, the problems already discussed above apply also to $H_2N(\alpha/\beta$–HNCO–$J)$). The first source is incomplete elimination of main-chain amides, which may overlap with the NH_2 correlations (*vide infra*). Second, the J-mismatch of the $^{1}J_{NCO}$ antiphase filter results in an inadequate separation of multiplet components. In our hands, the second-order NH_2 editing was adequate even in the anisotropic phase. It is worth emphasizing that even higher order NH_2 filtering can easily be utilized in the $H_2N(\alpha/\beta$–HNCO–$J)$ scheme without increasing overall length of the sequence. Regarding the purity of spin-state selection, the filter is quite insensitive to J-mismatch in the range 15 ± 3.5 Hz (*13*). If necessary, the incomplete suppression of multiplet components can be abolished by scaling the in- or antiphase data sets prior to Fourier transformation (*8*, *9*, *32*).

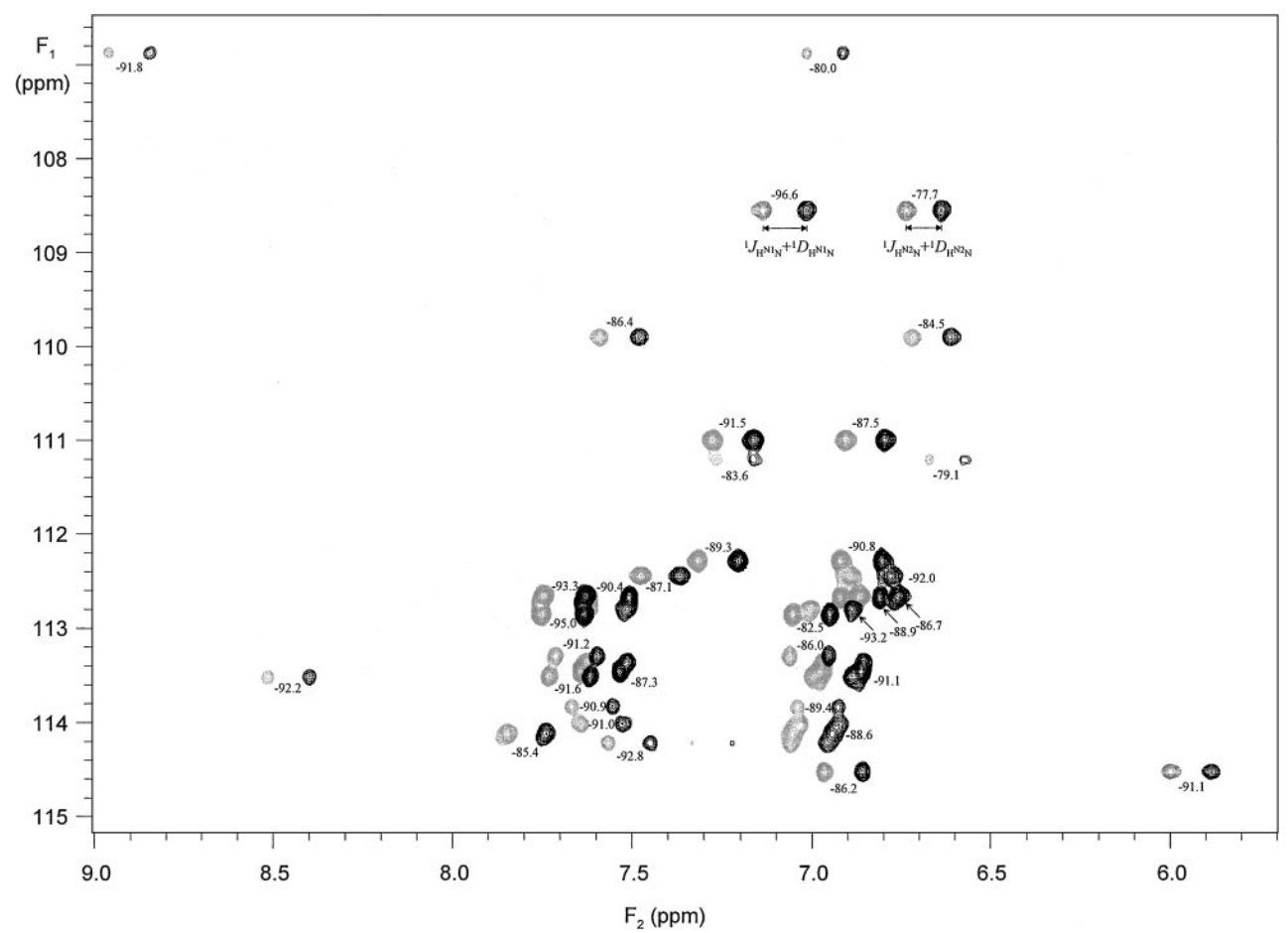

FIG. 2. Expansion of H_2N–HSQC–α/β–J spectrum, recorded from 0.5 mM uniformly ^{15}N-labeled Cel6A, in a dilute liquid crystal composed of filamentous Pf1 phages at 800 MHz ^{1}H frequency. The spectrum was collected with 128 and 1024 complex points using 8 transients per FID, which corresponds to acquisition times of 128 and 102 ms in t_1 and t_2, respectively. Data were zero-filled to 1024×4096 data matrices and apodized with shifted squared sine-bell functions in both dimensions. Up- (thick) and downfield (thin) multiplet components are shown overlaid. The measured couplings ($J + D$) in the anisotropic medium are indicated in the spectrum.

The proposed experiments were tested with two proteins: 0.5 mM uniformly ^{15}N-labeled Cel6A from the thermophilic soil bacterium *Thermobifida fusca* (286 amino acid residues, 30.4 kDa), dissolved in liquid crystal medium composed of Pf1 particles (13 mg/ml, the corresponding magnitude of alignment tensor was ~20 Hz) (*6*) 92/8% H_2O/D_2O, pH 6.0, 40°C, in a 350-μl Shigemi microcell; 0.9 mM U-^{15}N/^{13}C-enriched human cardiac troponin C (cTnC, 161 aa, 18 kDa), dissolved in 95/5% H_2O/D_2O in a 270-μl Shigemi microcell, pH 6.5, 40°C. The experiments were recorded on a Varian UNITY INOVA 800 NMR spectrometer, equipped with a ^{15}N/^{13}C/^{1}H triple-resonance probehead and an actively shielded triple-axis gradient system.

Figure 2 represents two overlaid subspectra recorded from Cel6A in a dilute liquid crystal phase using the proposed H_2N–HSQC–α/β–J experiment (Fig. 1a). Clean separation of ^{15}N–^{1}H multiplet components, as well as very good suppression of the main-chain amide correlation, is obtained, diminishing the partial overlap of cross peaks that may occur especially in larger proteins. The measured couplings ($J + D$) are marked on the spectrum. The figure clearly illustrates that the dipolar contribution to nonredundant N–H bond vectors can be very different, albeit motional averaging is likely to reduce this effect. The maximal $^{1}D_{NH}$ values found in backbone amides were ca. 20 Hz, compared with the values of ca. ±10 Hz measured in the side chains. This may reflect motional averaging or sparse orientation of NH_2 groups. Although clear indication of line broadening, arising from homonuclear dipolar contributions, was visible for a number of resonances, no splitting due to the homonuclear dipolar coupling between geminal protons was resolved in the F_2 dimension. In theory, maximal dipolar contributions between geminal protons yield values of ~15 Hz (assuming $r_{HH} = 1.8$ Å); however, in the case of a large, protonated protein, these are hardly resolved.

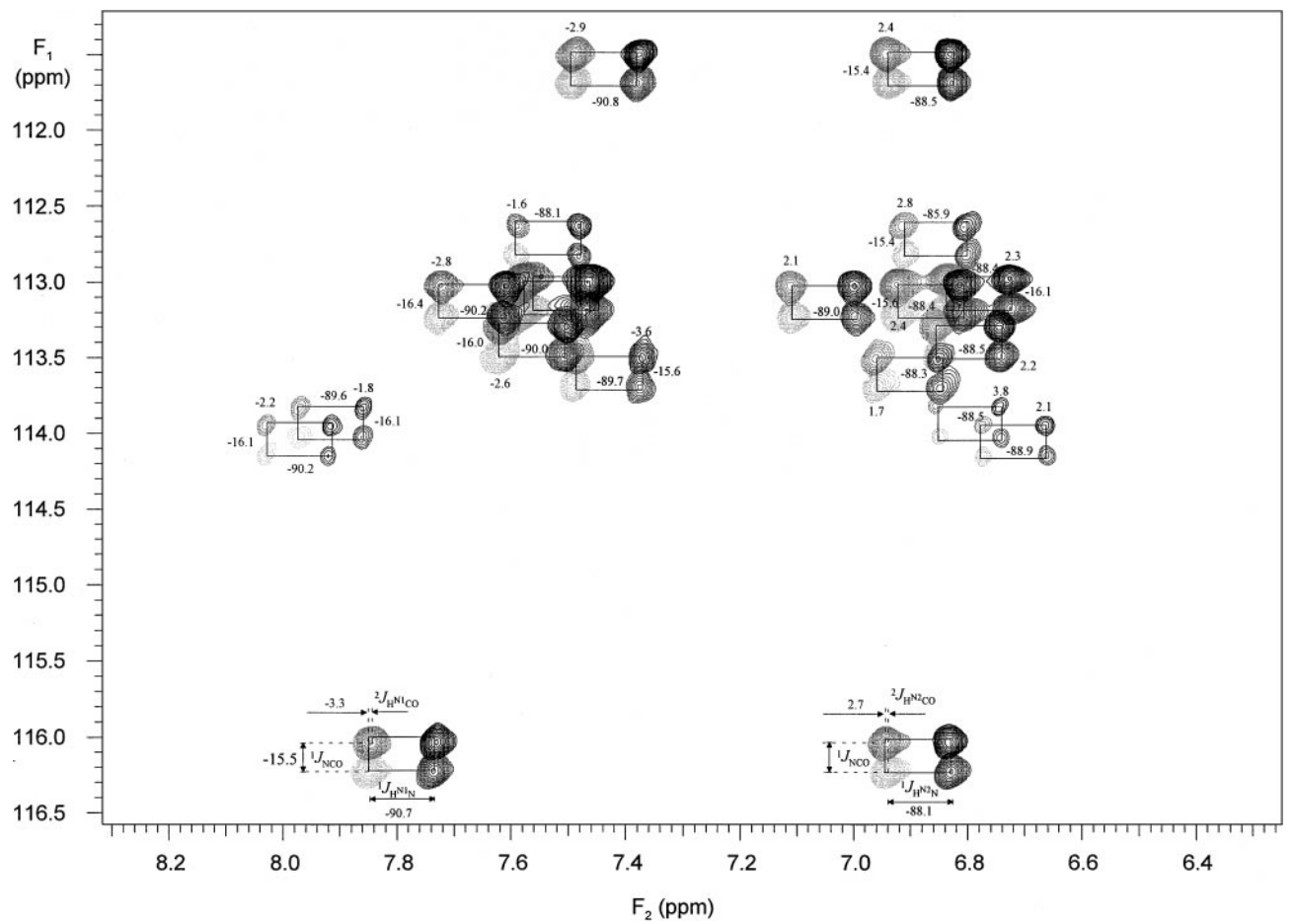

FIG. 3. Expansion of the NH_2 region of 0.9 mM U-^{13}C/^{15}N-labeled cTnC recorded using the H_2N(α/β–HNCO–J) scheme. The spectrum was recorded using 4 transients per FID with 128 and 512 complex points corresponding to acquisition times of 128 and 64 ms in t_1 and t_2, respectively. The data were postprocessed to a 4096 × 4096 matrix prior to Fourier transformation and phase-shifted squared sine-bell window functions were applied in both dimensions. Four different subspectra are superimposed. Each NH_2 cross peak is split in the F_1 (F_2) dimension by the $^{1}J_{NCO}$ ($^{2}J_{HNCO}$ and $^{1}J_{HN_N}$) couplings. The ^{15}N and (^{1}H) upfield and downfield components of the corresponding ^{13}CO–^{15}N ($^{1}H^{N}$–^{13}CO and ^{15}N–^{1}H) doublet components obtained by postacquisitional summation and subtraction of the in-phase and antiphase data sets are illustrated with different scales of gray color. The couplings measured from cTnC are indicated in the spectrum.

Figure 3 shows four overlaid F_1-^{13}CO and F_2-^{15}N, ^{13}CO coupled ^{15}N, ^{1}H subspectra of cTnC recorded using the $H_2N(\alpha/\beta$–HNCO–$J)$ pulse scheme. Cross peaks are displaced by the $^1J_{NCO}$ coupling in the F_1 dimension, and by the $^1J_{H^NN}$ and $^2J_{H^NCO}$ couplings in the F_2 dimension, as described above. The spectral simplification, obtained from spin-state selection, is clearly demonstrated, enabling the measurement of a larger number of couplings than would be possible using the conventional approach. The multiple measurement of the same coupling gave a precision of ±0.5, ±0.5, and ±0.2 Hz for the $^1J_{H^NN}$, $^2J_{H^NCO}$, and $^1J_{NCO}$ couplings, respectively. In the case of cTnC, all of the measured $^1J_{NCO}$ couplings varied between 15 and 16.5 Hz. A clear difference in the $^2J_{H^NCO}$ couplings can be found between the up- and downfield amide protons in all NH_2 moieties. The $^2J_{H^NCO}$ is negative and usually larger in magnitude for the downfield proton, whereas it is positive for the more shielded proton. In fact, this provides an alternative method for stereospecific assignment of NH_2 group to that proposed by McIntosh *et al.* (*34*). All measured ^{15}N–^{1}H couplings were between 86–91 Hz, indicating that $^1J_{H^NN}$ in side chains is somewhat smaller than in the protein main chain. Furthermore, the $^1J_{H^NN}$ couplings are a bit larger (more negative) for deshielded protons, which was observed already in 1976 by Bystrov (*35*).

In conclusion, we have described two new pulse sequences, which enable convenient and rapid measurement of $^1J_{H^NN}$, $^1J_{NCO}$, and $^2J_{H^NCO}$ couplings in the NH_2 side chains of Asn and Gln residues. The proposed experiments provide high sensitivity and resolution, which are essential for the precise measurement of couplings. The simultaneous editing with respect to the NH_2 moieties and spin-state selection facilitates the reduction of spectral width in the F_1 dimension owing to the limited number of cross peaks in the two-dimensional ^{15}N, ^{1}H correlation spectrum. Therefore, these experiments provide a wealth of structural information of NH_2 side chains obtained from high-quality spectra with relatively short experimental times.

ACKNOWLEDGMENTS

I thank Outi Salminen for providing the Cel6A sample, and Arto Annila and Jonathan Waltho for useful discussions. Finally, I thank the reviewers for their valuable comments and suggestions. This work was financially supported by the Ministry of Education.

REFERENCES

1. J. R. Tolman, J. M. Flanagan, M. A. Kennedy, and J. H. Prestegard, *Proc. Natl. Acad. Sci. USA* **92,** 9279–9283 (1995).
2. N. Tjandra and A. Bax, *Science* **278,** 1111–1114 (1997).
3. A. Bax and N. Tjandra, *J. Biomol. NMR* **10,** 289–292 (1997).
4. C. A. Bewley, K. R. Gustafson, M. R. Boyd, D. G. Covell, A. Bax, G. M. Clore, and A. M. Gronenborn, *Nat. Struct. Biol.* **5,** 571–578 (1998).
5. G. M. Clore, A. M. Gronenborn, and N. Tjandra, *J. Magn. Reson.* **131,** 159–162 (1998).
6. M. R. Hansen, L. Mueller, and A. Pardi, *Nat. Struct. Biol.* **5,** 1065–1074 (1998).
7. A. Annila, H. Aitio, E. Thulin, and T. Drakenberg, *J. Biomol. NMR* **14,** 223–230 (1999).
8. P. Permi, P. R. Rosevear, and A. Annila, *J. Biomol. NMR* **17,** 43–54 (2000).
9. M. Ottiger, F. Delaglio, and A. Bax, *J. Magn. Reson.* **131,** 373–378 (1998).
10. M. Cai, H. Wang, E. T. Olejniczak, R. P. Meadows, A. H. Gunasekera, N. Xu, and S. W. Fesik, *J. Magn. Reson.* **139,** 451–453 (1999).
11. D. Yang, J. R. Tolman, N. K. Goto, and L. E. Kay, *J. Biomol. NMR* **12,** 325–332 (1998).
12. D. Yang, R. A. Venters, G. A. Mueller, W. Y. Choy, and L. E. Kay, *J. Biomol. NMR* **14,** 333–343 (1999).
13. P. Permi, S. Heikkinen, I. Kilpeläinen, and A. Annila, *J. Magn. Reson.* **140,** 32–40 (1999).
14. P. Permi, T. Sorsa, I. Kilpeläinen, and A. Annila, *J. Magn. Reson.* **141,** 44–51 (1999).
15. P. Permi and A. Annila, *J. Biomol. NMR* **16,** 221–227 (2000).
16. M. Ottiger, F. Delaglio, J. L. Marquardt, N. Tjandra, and A. Bax, *J. Magn. Reson.* **134,** 365–369 (1998).
17. P. Permi, S. Heikkinen, I. Kilpeläinen, and A. Annila, *J. Magn. Reson.* **139,** 273–280 (1999).
18. T. Carlomagno, W. Peti, and C. Griesinger, *J. Biomol. NMR* **17,** 99–109 (2000).
19. I. Bertini, I. C. Felli, and C. Luchinat, *J. Biomol. NMR* **18,** 347–355 (2000).
20. A. Kaikkonen and G. Otting, *J. Am. Chem. Soc.* **123,** 1770–1771 (2001).
21. J. J. Chou and A. Bax, *J. Am. Chem. Soc.* **123,** 3844–3845 (2001).
22. G. Kontaxis and A. Bax, *J. Biomol. NMR* **20,** 77–82 (2001).
23. J. R. Tolman, J. M. Flanagan, M. A. Kennedy, and J. H. Prestegard, *Nat. Struct. Biol.* **4,** 292–297 (1997).
24. J. H. Prestegard, H. M. Al-Hashimi, and J. R. Tolman, *Quart. Rev. Biophys.* **33,** 371–424 (2000).
25. G. Bodenhausen and D. Ruben, *J. Chem. Phys. Lett.* **69,** 185–188 (1980).
26. D. Yang and K. Nagayma, *J. Magn. Reson. A* **118,** 117–121 (1996).
27. A. Meissner, J. Ø. Duus, and O. W. Sørensen, *J. Biomol. NMR* **10,** 89–94 (1997).
28. P. Andersson, J. Weigelt, and G. Otting, *J. Biomol. NMR* **12,** 435–441 (1998).
29. S. Grzesiek and A. Bax, *J. Biomol. NMR* **3,** 185–204 (1993).
30. T. M. Logan, E. T. Olejniczak, R. X. Xu, and S. W. Fesik, *J. Biomol. NMR* **3,** 225–231 (1993).
31. M. Goldman, *J. Magn. Reson.* **60,** 437–452 (1984).
32. A. Meissner, T. Schulte-Herbrüggen, and O. W. Sørensen, *J. Am. Chem. Soc.* **120,** 7989–7990 (1998).
33. E. de Alba, M. Suzuki, and N. Tjandra, *J. Biomol. NMR* **19,** 63–67 (2000).
34. L. P. McIntosh, E. Brun, and L. E. Kay, *J. Biomol. NMR* **9,** 306–312 (1997).
35. V. F. Bystrov, *Prog. NMR Spectrosc.* **10,** 41–81 (1976).
36. M. Piotto, V. Sauder, and V. J. Sklenar, *J. Biomol. NMR* **2,** 661–665 (1992).
37. S. Grzesiek and A. Bax, *J. Am. Chem. Soc.* **115,** 12593–12594 (1993).
38. L. Emsley and G. Bodenhausen, *Chem. Phys. Lett.* **165,** 469–476 (1990).
39. D. Marion, M. Ikura, R. Tschudin, and A. Bax, *J. Magn. Reson.* **85,** 393–399 (1989).
40. M. McCoy and L. Mueller, *J. Magn. Reson.* **99,** 18 (1992).